Nature Environment and Pollution Technology
An International Quarterly Scientific Journal

p-ISSN: 0972-6268
(Print copies up to 2016)
e-ISSN: 2395-3454

Vol. 25 | No. 1 | Article ID B4321 | 2026

Original Research Paper

https://doi.org/10.46488/NEPT.2026.v25i01.B4321

Open Access Journal

From Sea to Science: Unveiling the Diverse Biotechnological Applications of Marine Endophytic *Bacillus aerius*

Sathyananth M., Varna Vijayan and Leon Stephan Raj T.†

Plant Molecular Biology Research Unit (PMRU), Department of Botany, St. Xavier's College (Affiliated to Manonmaniam Sundaranar University, Abishekapatti, T.N.), Palayamkottai, T.N., India

†Corresponding author: Leon Stephan Raj T, leostephanraj@gmail.com

Abbreviation: Nat. Env. & Poll. Technol.
Website: www.neptjournal.com

Received: 10-03-2025
Revised: 21-04-2025
Accepted: 02-05-2025

Key Words:

Marine bacteria
Bioactivity
Nanoparticles
Dye degradation
Biotechnology

Citation for the Paper:

Sathyananth, M., Vijayan, V. and Leon Stephan, R. T., 2026. From sea to science: Unveiling the diverse biotechnological applications of marine endophytic *Bacillus aerius*. Nature Environment and Pollution Technology, 25(1), B4321. https://doi.org/10.46488/NEPT.2026.v25i01.B4321

Note: From 2025, the journal has adopted the use of Article IDs in citations instead of traditional consecutive page numbers. Each article is now given individual page ranges starting from page 1.

ABSTRACT

Marine endophytic bacteria are a promising source of bioactive compounds with diverse applications. This study investigated the multifunctional properties of *Bacillus aerius* PMRU2.8, isolated from the marine red alga *Gracilaria sp*. collected from the coastal region of Tamil Nadu, India. The bacterium demonstrated significant antimicrobial activity against multiple human pathogens, with its ethyl acetate extract containing bioactive compounds, including indoles and ketones. Molecular docking analysis revealed potential binding mechanisms of the compounds to bacterial proteins. Additionally, *B. aerius* efficiently synthesized silver nanoparticles (AgNPs) with enhanced antimicrobial efficacy compared with the crude extract. The bacterium also exhibited remarkable bioremediation capability, decolorizing up to 92.5% of the Direct Blue 6 azo dye within 48 h. Cytotoxicity assays confirmed the potential therapeutic applications of both the extract and the biosynthesized AgNPs. These findings highlight *B. aerius* as a valuable resource for pharmaceutical development, nanobiotechnology, and environmental remediation.

INTRODUCTION

Marine organisms constitute a rich source of diverse bioactive metabolites exhibiting antimicrobial, antifungal, antiviral, and anticancer activities (Zhang et al. 2019). These properties present significant potential for developing novel drugs and therapeutic agents. Investigating the diversity and ecological roles of marine bacteria associated with algal samples is of paramount importance (Kaur et al. 2023, Gu et al. 2023). These bacteria often inhabit extreme environments and possess unique metabolic adaptations, producing secondary metabolites for defense (Petersen et al. 2020, Karthikeyan et al. 2022). Recent studies have successfully isolated novel bioactive compounds from these marine bacteria, underscoring their potential as therapeutics (Machado et al. 2015, Brito et al. 2018). Algae-associated bacteria produce antibacterial, antiviral, and anticancer compounds. Research has demonstrated that extracts from these bacteria exhibit antimicrobial activity, including efficacy against methicillin-resistant *Staphylococcus aureus* (MRSA) (Kranjec et al., 2020). The development of new antibacterial drugs is imperative to address the increasing prevalence of antibiotic resistance (Butler et al. 2022). Silver nanoparticles (AgNPs) have demonstrated considerable promise as broad-spectrum antimicrobial agents because of their small size and high surface area. AgNPs synthesized using bacteria have been evaluated for their antimicrobial effects (Yin et al. 2020). However, the cytotoxicity of AgNPs remains a significant concern in biomedical applications. Textile dyes are a major source of global water pollution (Kishor et al. 2021). Azo dyes are particularly concerning because of their stability and resistance to degradation (Varjani et al. 2020). Bioremediation using microorganisms is a promising method for removing azo dyes from wastewater

(Chen et al. 2021). Bacteria capable of degrading azo dyes have been isolated from textile wastewater and textile sludge. However, degradation efficiency varies significantly depending on the bacterial strain and dye structure (Paba et al. 2021).

Despite these advances, a significant research gap exists in the comprehensive characterization of marine red algae-associated bacteria with multifunctional capabilities. While isolated studies have explored antimicrobial properties (Huang et al. 2023), nanoparticle synthesis, and dye degradation separately (Jamil et al. 2024), few investigations have systematically evaluated all these functionalities within the same bacterial isolates from marine red algae. Furthermore, the molecular mechanisms underlying these bioactivities, particularly through chemical profiling and in silico analysis of active compounds, remain insufficiently explored in this ecological niche on the southeast coast of Tamil Nadu.

Therefore, the present study aimed to isolate bacteria associated with marine red algae and systematically evaluate their multifaceted bioactive potential, including antimicrobial, dye decolorization, and cytotoxic activities. Additionally, this study investigated the biosynthesis of silver nanoparticles and conducted chemical profiling of antibacterial extracts from the isolates. These results provide insights into the biotechnological applications of algae-associated bacteria as sources of therapeutic natural products and environmentally sustainable processes.

MATERIALS AND METHODS

Isolation of Endophytic Bacteria

Marine bacteria associated with the red algae *Gracilaria* sp., collected from the rocky beach of Manapaadu, Tamil Nadu, India, were isolated and enumerated using a standardized serial dilution and plating technique (Shen & Zhang 2023). Algal tissues were surface sterilized and homogenized in sterile seawater (Mangun et al. 2023). The homogenate was serially diluted and subsequently plated onto Zobell Marine agar medium (Prabhakara & Kuehn 2023). Following a 72-hour incubation period at 27°C in the dark, bacterial colonies were enumerated, subcultured, and preserved as pure cultures.

Preliminary Screening

Isolates were cultured in Zobell marine broth for 96 h, and the fermented supernatant was collected from each culture. These supernatants were concentrated and subsequently assayed for antibacterial activity against human pathogens, including Escherichia coli, Klebsiella pneumoniae, Pseudomonas aeruginosa, Enterococcus faecalis, Serratia marcescens, Proteus mirabilis, Salmonella typhimurium, Staphylococcus aureus, Vibrio sp. and Aeromonas hydrophila, utilizing the paper disc diffusion method (Carvalho et al. 2018). Isolates demonstrating maximum antibacterial activity were selected for further experiments.

Polyphasic Recognition of Potential Isolates

Morphological Characterization: In accordance with Bergey's Manual of Determinative Bacteriology (Buchanan & Gibbons, 1974), colony morphology was evaluated on nutrient agar, encompassing shape, form, edge, elevation, and pigmentation of the colonies. Cell size and shape were observed microscopically at 10x and 100x magnification. Gram staining (Bullock & Aslanzadeh 2012) and the hanging drop method were utilized to determine Gram reaction and motility, respectively.

Molecular Identification of Bacterial Isolates: The Genomic DNA of the bacterial isolates was extracted using the Nucleo Spin Tissue kit. The 16S rRNA gene was amplified via PCR using universal primers P63f and P1378r, Phire PCR master mix, primers, water, and template DNA. The thermal cycling protocol comprised initial denaturation at 95°C for 5 min, followed by 35 cycles of denaturation (95°C, 40 s), annealing (60°C, 40 s), extension (72°C, 60 s), and a final extension at 72°C for 7 min. Amplification was confirmed by agarose gel electrophoresis with ethidium bromide staining and UV imaging. Sequencing was performed using the Big Dye Terminator v3.1 kit on an ABI 3500 genetic analyzer, with quality assessment conducted via Sequence Scanner v1 and alignment performed using Geneious Pro v5.1. Identification was accomplished through a BLAST search against the NCBI GenBank database, confirming 100% sequence similarity to the prototype strains.

Secondary Metabolite Extraction and Spectroscopy Evaluation from Potent Isolates

The bacterial isolate was cultured in starch casein media at 29°C with agitation for 48 h. Subsequently, a 2% inoculum was transferred to fresh production media (8 L) and incubated under similar conditions for 8-12 days. Following fermentation, the biomass was separated via filtration. The filtrate was combined with ethyl acetate, and after overnight agitation, the bioactive compounds partitioned into the organic layer (Xie et al. 2021). The organic layer was subsequently collected and concentrated using a vacuum rotary evaporator to remove ethyl acetate, resulting in purified bioactive compounds. Gas chromatography-mass spectrometry (GC-MS) and Fourier-transform infrared spectroscopy (FTIR) were employed to identify the antimicrobial compounds and functional groups,

facilitating their characterization.

Molecular Docking Analysis

Molecular docking simulations were conducted using Auto-Dock Vina. Ligand structures were obtained from PubChem. The sdf format underwent energy minimization using the ChemBio3D software. The three-dimensional structures of the receptor proteins (PDB ID: 3K8E, 1N67, and 1T2P) were obtained from the Protein Data Bank and prepared by eliminating co-crystallized ligands, water molecules, and cofactors. Auto-Dock 4.2 (MGL tools 1.5.6) prepared files, and Auto-Dock Vina was used to execute the docking simulations. The docking grid encompassed the entire protein target area, exploring nine ligand conformations. Ligand-receptor interactions were analyzed, with an emphasis on favorable binding energies and key residues, using Discovery Studio Visualizer in three-dimensional formats.

ADMET Analysis

Using the Swiss ADME online tool, computational predictions of citronellal and terpinen-4-ol ADME, drug-likeness, and pharmacokinetics were conducted. The following physicochemical parameters and ADME features were determined: molecular weight (MW), hydrogen bond acceptor (HBA), hydrogen bond donor (HBD), topological polar surface area (TPSA), octanol/water partition coefficient (LogP), and rotatable bond count (RB).

Silver Nanoparticle Biosynthesis

Silver nanoparticles were synthesized utilizing cell-free supernatants of a potent bacterial isolate cultured in Zobell marine broth 2216 (Ghodake et al. 2020). The broth was centrifuged, and the resulting supernatant was combined with 1mM silver nitrate solution in a 1:10 ratio. The formation of AgNPs was indicated by a color change from white to brown and subsequently confirmed through UV-vis spectroscopy using a Shimadzu UV1800 spectrophotometer, with spectra recorded from 200-1100 nm at 24-h intervals. The nanoparticles were characterized by centrifugation at 5000 rpm, followed by washing with ethanol and drying for SEM analysis (Chakraborty et al. 2023).

Antibacterial Activity

The antibacterial activity of the ethyl acetate extracts and AgNPs of the selected isolates was evaluated using the disc diffusion assay (Bauer et al. 1966) against clinically isolated bacterial pathogens obtained from the Scudder Microbiology Laboratory, Nagercoil, India. Mueller-Hinton agar plates were inoculated with pathogen cultures grown to a 0.5 McFarland standard. Filter paper discs were impregnated with extracts, silver nanoparticles, positive control (ampicillin), and negative controls (DMSO and ethyl acetate). The plates were incubated at 37°C for 18-24 h, and the inhibition zones were measured (Bauer et al. 1966). The percentage of inhibition was calculated using Equation (1).

$$PI = \frac{100 \times (X - Y)}{(Z - Y)} \quad ...(1)$$

Where X = Mean test extract,

Y = Mean negative control,

Z = Mean positive control.

Azo Dye Degradation

Several azo dyes have been evaluated for biodegradation by marine bacteria. The dyes examined included Brilliant Green ($C_{27}H_{34}N_2O_4S$, CAS: 633-03-4, λ max- 244 nm), Sudan black B ($C_{29}H_{24}N_6$, CAS: 4197-25-5, λ max- 454 nm), Direct Blue 6 ($C_{32}H_{20}N_6Na_4O_{14}S_4$, CAS: 2602-46-2, λ max- 566 nm), and Disperse Red 1 ($C_{16}H_{18}N_4O_3$, CAS: 2872-52-8, □ max- 480 nm). Zobell marine broth 2216 was prepared (30 mL.tube^{-1}), sterilized, and inoculated with the bacterial isolate. Dye degradation experiments were conducted by adding dyes (2 mg.mL^{-1}) to 24 h cultures. The decolorization was visually monitored. Cell-free supernatants were analyzed using UV-vis spectrophotometry on a Shimadzu UV 1800 instrument. The maximum absorbance wavelengths were determined by scanning from 200 to 1100 nm. Abiotic and uninoculated controls were also included. The decolorization percentage and average rates were calculated using Equations (2) and (3), respectively.

$$\text{Percentage of decolorization} = \frac{(Initial\ absorbance - Final\ absorbance)}{Initial\ absorbance} \times 100 \quad ...(2)$$

$$\text{Average decolorization rate} = \frac{C \times \%D}{100 \times t}\ \text{mg/L/h} \quad ...(3)$$

Where C is the initial dye concentration,

% D is the percentage of dye decolorized after time t.

Brine Shrimp Lethality Bioassay

The cytotoxicity of the bacterial extracts was evaluated using the brine shrimp lethality assay (Meyer et al., 1982). Brine shrimp larvae were hatched in artificial seawater under oxygenation conditions. Groups of 10 nauplii were subjected to varying concentrations (1-1000 µg.mL^{-1}) of ethyl acetate extract (EAE) and silver nanoparticles (AgNPs) from the potent isolate B. aerius PMRU2.8 dissolved in seawater with 1% DMSO. Each concentration was replicated three times, with 1% DMSO serving as the negative control. After 24 h, the surviving nauplii were enumerated, and the percentage

mortality was calculated, adjusting for control mortality. The median lethal concentration (LC_{50}) was determined through probit analysis using the SPSS software (version 22, IBM Corp.). For the analysis, mortality percentage data were plotted against the logarithm of the concentration, and linear regression analysis was performed to generate the regression equations. The LC_{50} values were calculated by interpolating the 50% mortality point on these regression lines. An LC_{50} value exceeding 1000 $\mu g.mL^{-1}$ was considered indicative of non-toxicity.

A schematic of the experimental pipeline is shown in Fig. 1.

RESULTS AND DISCUSSION

Preliminary Screening

A total of 48 bacterial strains were isolated as endophytes from the marine red alga *Gracilaria* sp. and evaluated for their antimicrobial activity against human pathogens. The isolates exhibiting inhibitory activity against the pathogens are listed in Table 1, which indicates that isolate MR-60 demonstrated superior activity among the isolates. The morphological and biochemical characteristics of these potent isolates are systematically presented in Table 2.

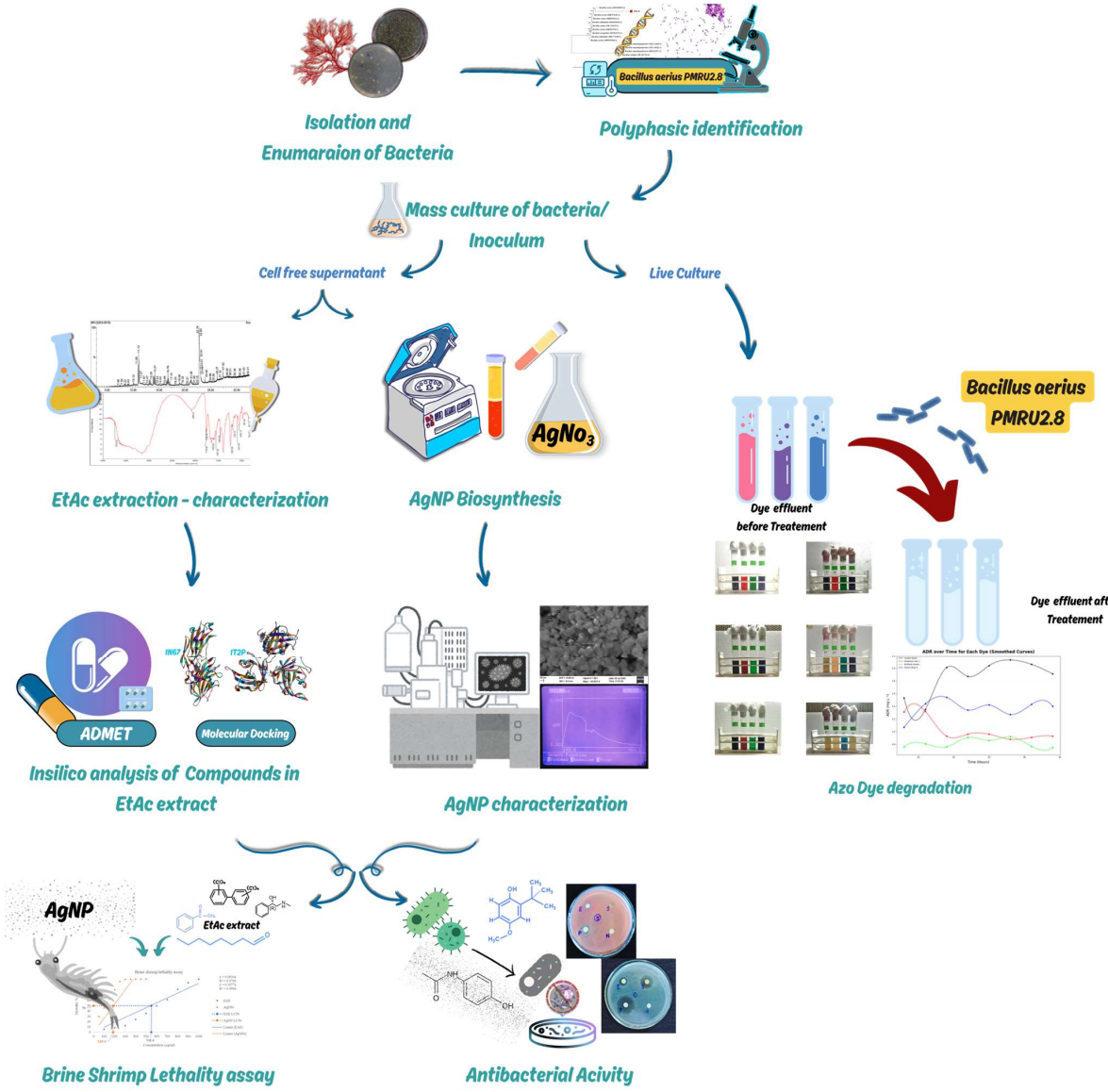

Fig. 1: Schematic Diagram of the Experimental Pipeline.

Table 1: Preliminary screening of potent isolates.

Pathogens	MR 08	MR 14	MR 26	MR 32	MR 39	MR 41	MR 53	MR 60	MR 63	MR 65
Escherichia coli	++	-	-	-	-	+	+	+++	-	+
klebsiella pneumoniae	+	-	-	-	+	-	-	+++	+	-
Pseudomonas aeruginosa	-	+++	++	-	++	+++	+	-	++	-
Enterococcus faecalis	-	+	-	++	+	-	-	++	-	+
Serratia marcescens	-	-	-	+	+	+	-	-	-	+
Proteus mirabilis	+	-	+++	+	-	+	-	+++	-	-
Salmonella typhimurium	-	+++	-	++	-	+	+++	+	+	-
Staphylococcus aureus	-	-	-	-	-	+++	-	+	-	-
Vibrio sp.	+	+	+++	-	+	-	+	++	-	+
Aeromonas hydrophila	+	-	+	-	+++	-	+	++	+	-
Total	5	4	4	4	6	6	5	8	4	4

'+++' – High activity, '++' Medium activity, '+'low activity, '-no activity.

Table 2: Morphological and Biochemical Characterizations.

Isolates	MR 08	MR 14	MR 26	MR 32	MR 39	MR 41	MR 53	MR 60	MR 63	MR 65
Morphology										
Gram's stain	-	-	+	-	+	+	-	+	-	+
Motility	+	-	+	-	-	+	+	+	+	+
Pigment	White	White	White	Yellow	Gray	White	White	White	White	White
Shape	Rod	Rod	Rod	Rod	Rod	Rod	Rod	Rod	Rod	Rod
Biochemical tests										
Indole	+	-	-	-	-	-	-	-	-	-
Methyl red	-	-	+	-	-	-	-	-	-	-
Voges Poskauer	-	-	-	-	-	-	-	+	+	-
Citrate	+	+	+	-	-	-	+	+	+	-
Oxidase	+	+	-	+	-	-	-	-	+	+
Catalase	+	+	+	+	+	+	+	+	+	+
H_2S Production	-	-	+	-	-	-	-	+	-	+
Starch	-	-	-	-	+	-	-	+	+	+
Nitrate reduction test	-	+	+	+	+	+	-	+	+	-
Gelatinase	+	+	-	-	+	-	-	+	-	-
Sugar Utilization										
Sucrose	+	+	-	+	+	+	-	+	+	+
Glucose	+	+	-	+	+	-	-	+	-	-
Rhamnose	-	-	-	-	-	-	-	-	-	-
Maltose	-	+	-	+	+	+	-	+	+	-
Lactose	+	+	-	-	+	+	-	-	+	-
Mannitol	+	+	-	+	+	+	-	+	-	-
Identified organisms	*Vibrio* sp.	*Aeromonas* sp.	*Bacillus* sp.	*Pseudomonas* sp.	*Clostiridium* sp.	*Lactobacillus* sp.	*Acinetobacter* sp.	*Bacillus* sp.	*Photobacterium* sp.	*Lysinibacillus* sp.

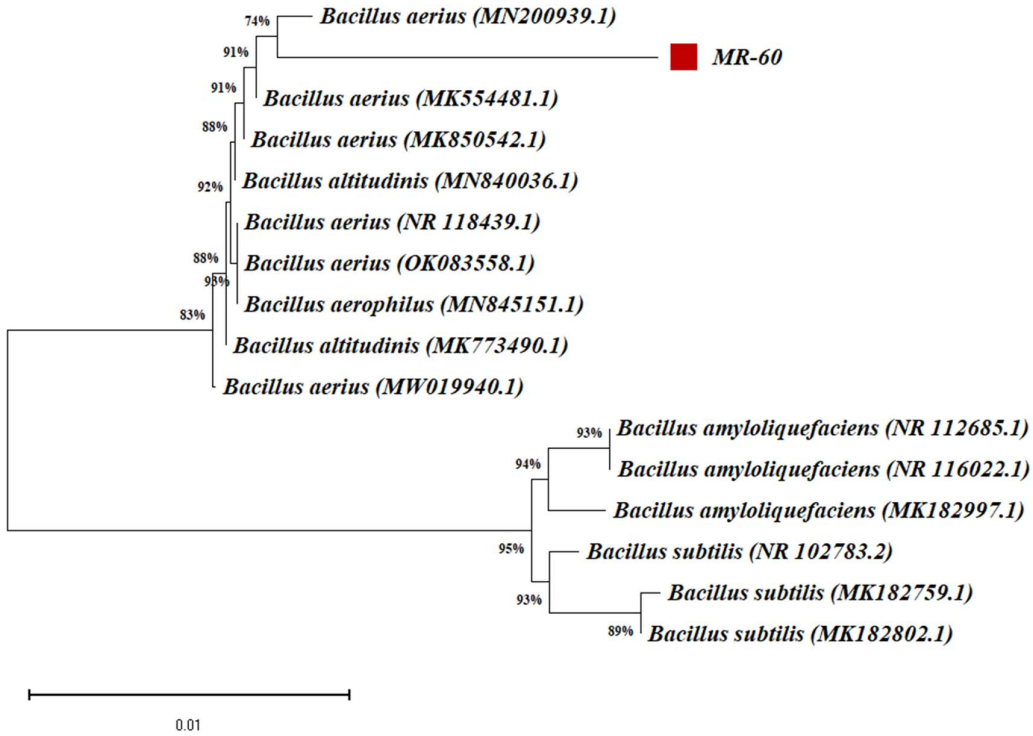

Fig. 2: Phylogenetic analysis of B. aerius PMRU2.8.

Molecular identification of the isolate exhibiting the highest activity, MR-60, was performed through 16S rRNA gene sequencing. The sequence exhibited maximum similarity to *Bacillus aerius* strain 24 K (MN200939.1), with 100% query coverage and 98.12% identity. Phylogenetic analysis indicated that isolate MR-60 formed a closely related clade with *Bacillus aerius* type sequences, whereas *B. subtilis* and B. *amyloliquefaciens* served as outgroups (Fig. 2). Based on phenotypic, biochemical, and molecular characterization, isolate MR-60 was confirmed to be *Bacillus aerius*. The sequence was subsequently submitted to the NCBI with the GenBank accession number PP415878 as *Bacillus aerius* PMRU2.8.

Analysis of Ethyl Acetate Extract of *B. aerius* PMRU2.8

The ethyl acetate extract of *B. aerius* PMRU2.8 was analyzed using FTIR spectroscopy and GC-MS, revealing a diverse chemical profile (Table 3, Figs. 3 & 4). FTIR spectroscopy identified key functional groups (carboxylic acids, ketones, esters, aromatics, and alkanes), whereas GC-MS confirmed the presence of specific compounds, including heterocyclic aromatics (indole, 2,5-dimethylpyrazine), ketones, esters, carboxylic acids, sulfur compounds (dimethyl disulfide), and alkanes (octadecane). Several compounds, particularly indole derivatives and nitrogen-containing aromatics,

Table 3: Analysis of Ethyl Acetate Extract of B. aerius PMRU2.8.

CID	GCMS		FT-IR	
	Compound Name	Mol. Formula - Mol. Weight	Functional Group	Wavenumber Range with Bond Stretch
798	Indole	C_8H_7N - 117.15	Aromatic Amine	1450-1600 (C=C), 3300-3500 (broad, N-H)
31252	2,5-Dimethylpyrazine	$C_6H_8N_2$ - 108.14	Aromatic ring - N	1450-1600 (C=C)
8034	5-Methyl-2-hexanone	$C_7H_{14}O$ - 114.19	Ketone	1700-1750 (C=O)
12232	Dimethyl disulfide	$C_2H_6S_2$ - 94.2	Sulfide	600-700 (C-S)
24020	Ethyl 2-methylbutanoate	$C_7H_{14}O_2$ - 130.18	Ester	1720-1770 (C=O), 1200-1300 (C-O)
10430	3-Methyl-butanoic acid	$C_5H_{10}O_2$ -102.13	Carboxylic acid	2500-3300 (broad, O-H), 1700-1750 (C=O)
7909	Methyl isobutyl ketone	$C_6H_{12}O$ - 100.16	Ketone	1700-1750 (C=O)
11635	Octadecane	$C_{18}H_{38}$ - 254.5	Alkane	2800-2950 (C-H)

possess antimicrobial properties. This chemical diversity demonstrates the complex metabolic capabilities of the isolate and suggests potential applications in the agricultural, pharmaceutical, and industrial fields.

Molecular Docking Analysis

Molecular docking analysis was used to assess the binding affinities of the eight volatile compounds against three bacterial proteins critical for pathogenesis (Table 4). For CMP-Kdo synthetase (PDB ID: 3K8E), indole exhibited the strongest binding, with a docking score of -6.3, whereas dimethyl disulfide showed the weakest interaction, with a score of -2.0. In the case of Clumping Factor A (PDB ID: 1N67), indole again demonstrated superior binding affinity with a score of -7.0, while 3-methyl-butanoic acid had the highest score of -4.6, indicating weaker binding. Regarding SrtA (PDB ID: 1T2P), octadecane displayed the strongest binding affinity with a score of -6.3, whereas 2,5-dimethylpyrazine exhibited the weakest interaction with a score of -4.2. These findings suggest that indole may inhibit CMP-Kdo synthetase and Clumping Factor A, whereas octadecane shows potential as a Sortase A inhibitor. Conversely, dimethyl disulfide demonstrated poor binding affinity for all targets, indicating its limited antimicrobial potential.

ADMET Analysis

Ethyl 2-methylbutanoate demonstrated the highest number of hydrogen bond acceptors (HBA: 5) and donors (HBD: 1), indicating favorable solubility and binding properties. However, its topological polar surface area (TPSA: 72.83 Å²) may restrict membrane permeability. Octadecane exhibited significant lipophilicity (LogP: 7.18) but limited aqueous solubility, along with a substantial number of rotatable bonds (Rb: 15), suggesting its structural flexibility. Dimethyl disulfide and ethyl 2-methylbutanoate both presented a relatively high TPSA (50.60 Å²), whereas

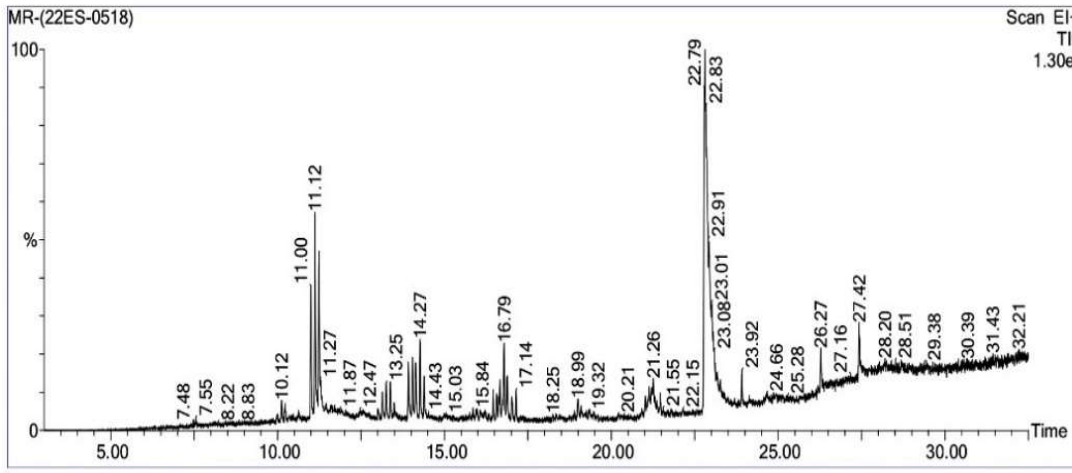

Fig. 3: GC-MS Analysis of Ethyl Acetate Extract.

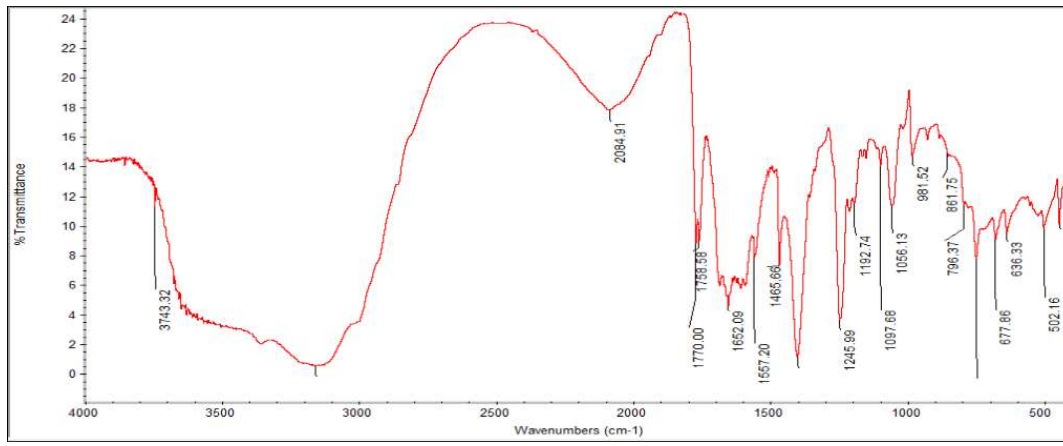

Fig. 4: FT-IR Analysis of Ethyl Acetate Extract.

Table 4: Molecular Docking Analysis of Compounds in Ethyl Acetate Extract of *B. aerius* PMRU2.8.

Compounds	3K8E	1N67	1T2P
2-5-Dimethylpyrazine	-4.6	-5.1	-4.2
3-Methyl-butanoic_acid	-4.2	-4.6	-4.2
5-Methyl-2-hexanone	-4.6	-4.5	-5.7
Dimethyl_disulfide	-2.0	-2.4	-1.9
Ethyl_2-methylbutanoate	-4.3	-4.5	-5.2
Indole	-5.3	-7.0	-6.3
Methyl_isobutyl_ketone	-4.2	-4.3	-4.0
Octadecane	-4.3	-5.3	-6.3

indole and 2,5-dimethylpyrazine showed lower TPSA values, implying enhanced membrane permeability. These findings underscore the structural diversity and physicochemical properties that affect the pharmacokinetic behavior of these compounds (Table 5).

Silver Nano Particle Biosynthesis

The synthesis of AgNPs was achieved through the reduction of silver nitrate by *B. aerius* PMRU2.8, as evidenced by the color transition from yellow to white over a 24-h period. UV-vis spectroscopy identified an absorption peak at 445 nm, corroborating the formation of spherical nanoparticles. The observed blue shift in the peak position indicated a reduction in nanoparticle size. SEM analysis further substantiated the synthesis of silver nanoparticles, revealing an average diameter of approximately 150 nm with a uniform orientation centered around 340 degrees (Fig. 5).

Antibacterial Activity

The antibacterial efficacy of *B. aerius* PMRU2.8 ethyl acetate extract and its Silver Nanoparticles (SNPs) was assessed against ten bacterial pathogens (Table 6). SNPs (25 µg) exhibited superior inhibitory effects compared to the crude extract (100 µg) in 9 out of 10 pathogens tested.

Table 5: ADMET analysis of Ethyl acetate extract.

Compound name	HBA	HBD	TPSA	Log P	Rb
Indole	0	0	15.79 Å²	1.98	0
2,5-Dimethyl pyrazine	2	0	25.78 Å²	0.99	0
5-Methyl-2- hexanone	1	0	17.07 Å²	1.87	3
Dimethyl disulfide	0	0	50.60 Å²	1.34	1
Ethyl 2-methylbutanoate	5	1	72.83 Å²	3.88	7
3-Methylbutanoic acid	2	1	37.30 Å²	0.98	2
Methyl isobutyl ketone	1	0	17.07 Å²	1.48	2
Octadecane	0	0	0.00 Å²	7.18	15

HBA - Hydrogen Bond Acceptor, HBD - Hydrogen Bond Donor, TPSA - Topological Polar Surface Area, Log P- Lipophilicity, Rb - Rotatable bond.

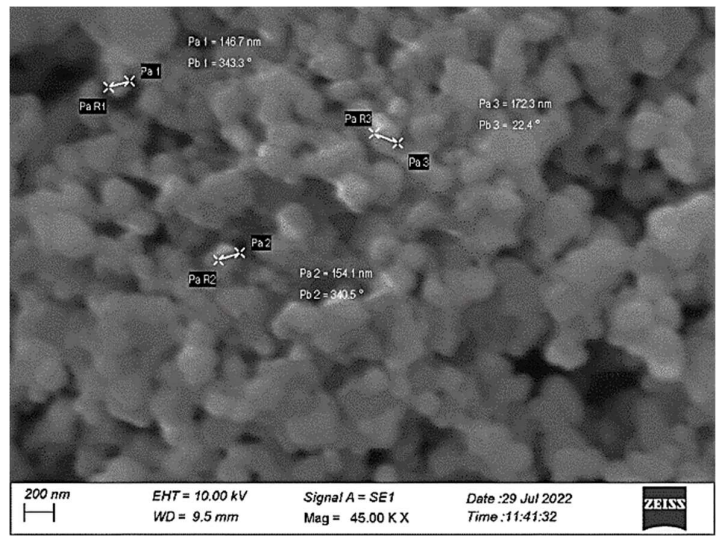

Fig. 5: SEM photograph of *B. aerius* PMRU2.8 synthesized SNP.

Inhibition zones for SNPs ranged from 7.83 to 23.8 mm, while those for the ethyl acetate extract ranged from 8.1 to 18.5 mm. Enterococcus faecalis showed the highest susceptibility to SNPs, with an inhibition zone of 23.8 mm (99.2% inhibition relative to streptomycin). Klebsiella pneumoniae also exhibited notable sensitivity to SNPs, with a mean inhibition zone of 20.5 mm (86.7% inhibition). Vibrio sp. was the only pathogen more sensitive to the crude extract (18.5 mm, 84.0% inhibition) than SNPs (17.1 mm, 77.6% inhibition). Statistical analysis confirmed significant

Table 6: Antibacterial activity of Ethyl acetate extract of *B. aerius* PMRU2.8 and its Silver Nano Particles.

S. No.	Pathogen	Samples	Zone Of Inhibition [mm]	Percentage of inhibition [%]
1	*Escherichia coli*	E	9.00 ± 0.54 a	35.9
		S	16.8 ± 0.41 bcd	69.7
		P	23.8 ± 0.86 b	-
		N	0.66 ± 0.30 a	-
2	*klebsiella pneumoniae*	E	11.8 ± 0.39 bc	48.3
		S	20.5 ± 0.25 e	86.7
		P	23.5 ± 0.68 b	-
		N	0.83 ± 0.40 a	-
3	*Pseudomonas aeruginosa*	E	8.5 ± 0.38 a	33.8
		S	15.3 ± 0.26 b	63.3
		P	23.8 ± 0.80 b	-
		N	0.66 ± 0.54 a	-
4	*Enterococcus faecalis*	E	12.1 ± 0.40 c	47.4
		S	23.8 ± 0.15 cde	99.2
		P	24 ± 0.31 b	-
		N	1.5 ± 0.15 a	-
5	*Serratia marcescens*	E	8.8 ± 0.25 a	60.2
		S	7.83 ± 0.15 a	52.6
		P	13.8 ± 0.41 a	-
		N	1.16 ± 0.41 a	-
6	*Proteus mirabilis*	E	8.8 ± 0.15 a	34.1
		S	21.5 ± 0.40 e	92.3
		P	23.1 ± 1.17 b	-
		N	1.33 ± 0.55 a	-
7	*Salmonella typhimurium*	E	8.1 ± 0.15 a	34.5
		S	19.5 ± 0.54 de	85.1
		P	22.8 ± 0.68 b	-
		N	0.33 ± 0.83 a	-
8	*Staphylococcus aureus*	E	10.3 ± 0.30 abc	40.1
		S	16.16 ± 0.40 bc	64.5
		P	24.6 ± 0.15 b	-
		N	0.66 ± 0.55 a	-
9	*Vibrio* sp.	E	18.5 ± 0.26 d	84.0
		S	17.1 ± 0.41 bcd	77.6
		P	21.8 ± 0.85 b	-
		N	1 ± 0.53 a	-
10	*Aeromonas hydrophila*	E	9.66 ± 0.79 ab	43.5
		S	14 ± 0.53 b	64.5
		P	21.3 ± 0.79 b	-
		N	0.66 ± 0.3 a	-

E- Ethyl acetate extract (100 µg), S- Silver Nanoparticle (25 µg), P- Positive control (Streptomycin 10 µg), N-Negative control (Ethyl acetate-100 µL). Statistics: dF = 9,1 (ESPN), p =>0.001(ESPN), F= (E=42.175), (S=37.404), (P=17.921) (N =0.995)

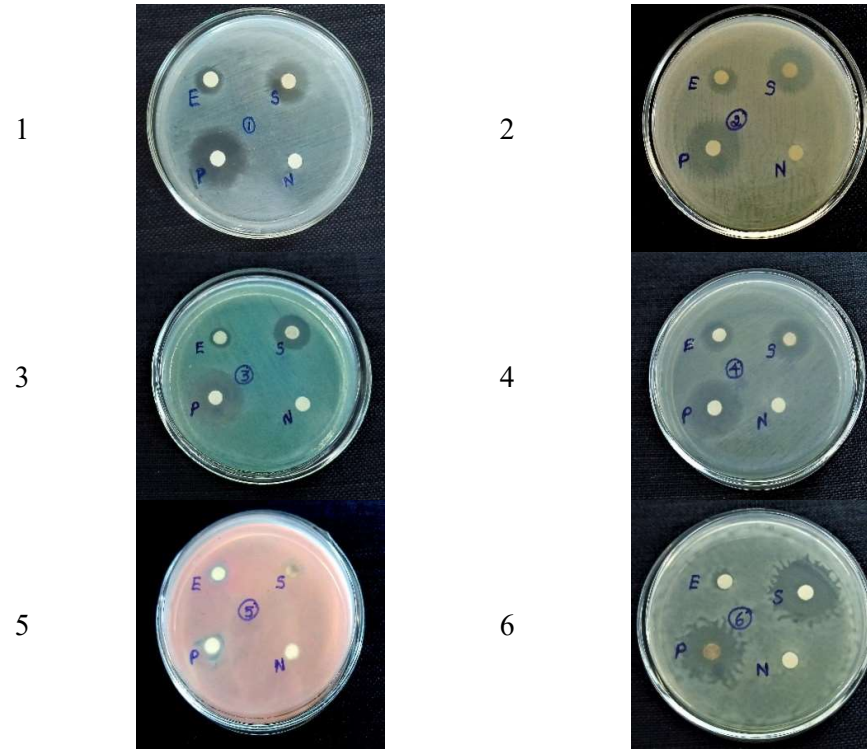

E- Ethyl acetate extract (100 µg),
S- Silver Nanoparticle (25 µg),
P- Positive control (Streptomycin 10 µg),
N-Negative control (Ethyl acetate-100 µL).

Fig. 6: Antibacterial activity of Ethyl acetate extract and SNP of B. aerius PMRU2.8.

Table 7: Azo-Dye degradation of B. aerius PMRU2.8.

Time (Hrs)	Sudan Black		Disperse red 1		Brilliant Green		Direct Blue 6	
	%D	ADR	%D	ADR	%D	ADR	%D	ADR
0	0	-	0	-	0	-	0	-
6	9.18 ± 2.03	1.53	12.1 ± 2.26	1.31	9.26 ± 1.26	0.76	12 ± 1.25	1.07
12	16.3 ± 1.26	1.35	21.6 ± 1.02	1.32	17.6 ± 3.25	0.81	25.4 ± 2.25	1.44
18	36.2 ± 1.02	2.01	33.7± 1.03	0.93	25.8 ± 2.02	0.76	39.8 ± 1.25	1.54
24	45.1 ± 3.26	1.87	43.7 ± 1.03	0.96	39.8 ± 1.65	0.91	53.6 ± 1.54	1.34
30	61.3 ± 1.02	2.04	59.3 ± 3.26	0.96	51.2 ± 1.26	0.86	72.7 ± 2.02	1.42
36	76.9 ± 3.02	2.13	67.7 ± 1.02	0.88	61.8 ± 2.65	0.92	79.9 ± 1.52	1.27
42	86.9 ± 1.00	2.06	79.4 ± 2.15	0.91	62.9 ± 3.29	0.77	88.9 ± 3.59	1.43
48	91.9 ± 2.03	1.91	86.2 ± 1.02	0.93	65.3 ± 1.26	0.75	92.5 ± 1.25	1.40

% D – Percentage of Colorization, ADR – Average colorization rate (mg L^{-1})

differences between treatments ($p<0.001$), with F-values of 42.175, 37.404, and 17.921 for the extract, SNPs, and positive control, respectively (Fig. 6).

Azo Dye Degradation

The bacterial isolate *B. aerius* PMRU2.8 showed notable decolorization capabilities against four distinct azo dyes over 48 h, as shown in Table 7 and Fig. 7 & Fig. 8 . Direct Blue 6 had the highest decolorization rate, achieving 92.5% after 48 h, with an average decolorization rate (ADR) of 1.40 $mg.L^{-1}$. Sudan Black followed with 91.9% decolorization and an ADR of 1.91 $mg.L^{-1}$. Disperse Red 1 reached 86.2%

decolorization with an ADR of 0.93 mg.L^{-1}, while Brilliant Green had the lowest at 65.3% with an ADR of 0.75 mg.L^{-1}. The decolorization process was time-dependent for all dyes. Initial rates were slow, with only a 9.18-12.1% reduction after 6 h. A significant increase occurred between 18-36 h. For Sudan Black, decolorization rose from 36.2% at 18 h to 76.9% at 36 h. Similarly, Direct Blue 6 increased from 39.8% at 18 h to 79.9% at 36 h. The rate plateaued between 42-48 h for most dyes, indicating nearing maximum decolorization capacity. ADRs varied significantly, with Sudan Black consistently showing the highest ADR, reaching 2.13 mg L^{-1} at 36 h, while Brilliant Green consistently had the lowest ADR, never exceeding 0.92 mg L^{-1}.

Brine Shrimp Lethality Bioassay

The brine shrimp lethality assay (BSLA) was employed to assess the cytotoxic potential of *B. aerius* PMRU2.8 samples, specifically the ethyl acetate extract (EAE) and

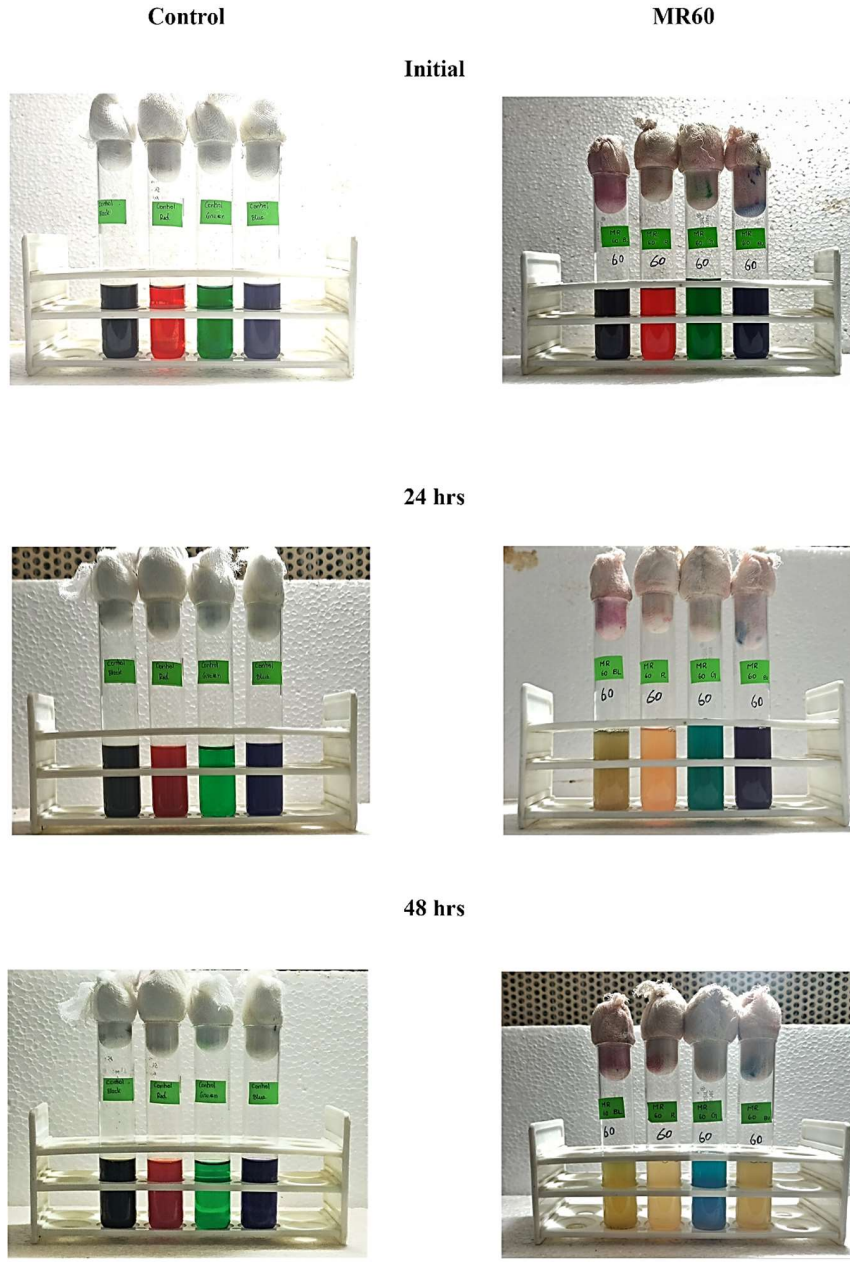

Fig. 7: Azo-Dye degradation assay of *B. aerius* PMRU2.8.

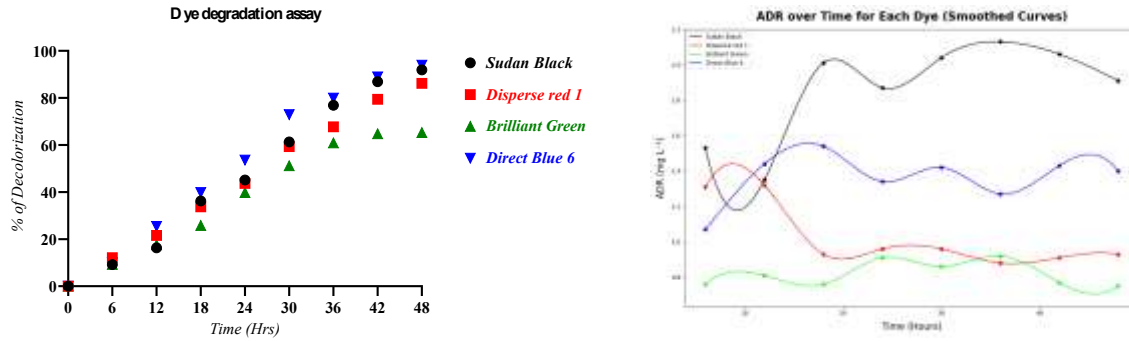

Fig. 8: Azo-Dye degradation assay of B. aerius PMRU2.8.

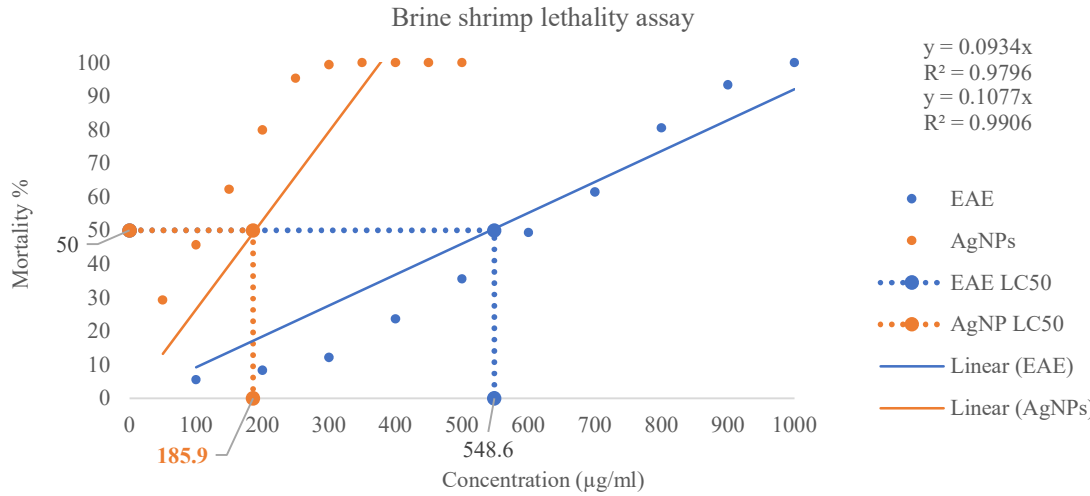

Fig. 9: Brine shrimp lethality bioassay.

silver nanoparticles (AgNPs) (Fig. 9). The assay results indicated variations in cytotoxicity among the samples. The AgNPs exhibited a higher level of cytotoxic activity, with an LC50 value of 310 µg.mL^{-1}, whereas the EAE exhibited moderate cytotoxicity, with an LC50 value of 548.6 µg.mL^{-1}. This finding suggests that AgNPs were approximately 1.77 times more potent than the crude extract in the brine shrimp lethality model. The lower LC50 value of the AgNPs indicates that a smaller concentration was necessary to achieve 50% mortality of the brine shrimp nauplii compared to the EAE, thereby demonstrating the enhanced cytotoxic potential of the nanoparticle formulation.

DISCUSSION

The ethyl acetate extract of *B. aerius* PMRU2.8 contains bioactive compounds with antibacterial properties. Indole derivatives affect E. coli and S. aureus via aromatic amine interactions (Bhagat et al. 2019). 5-methyl-2-hexanone inhibits S. aureus and Klebsiella pneumoniae by disrupting their membranes (Zhang et al. 2010). Carboxylic acids, such as 3-methylbutanoic acid, cause cytoplasmic acidification and membrane damage (Kim et al. 2012). Alkanes, such as octadecane, compromise membrane integrity (Malanovic et al. 2020).

Molecular docking analysis highlighted volatile compounds, particularly indole and octadecane, as potential inhibitors of bacterial proteins. The strong binding of indole to CMP-Kdo synthetase suggests interference with lipopolysaccharide biosynthesis in gram-negative bacteria, compromising cell wall integrity (Raetz & Whitfield 2002). This finding supports the study by Gao et al. (2018), which focused on bacterial growth inhibition through CMP-Kdo synthetase targeting. Indole also binds strongly to Clumping Factor A in Staphylococcus aureus, disrupting adherence and biofilm formation, supporting Fernandez-Calvo et al.'s (2024) findings. Ganesh et al.'s (2008) model reinforces ClfA-fibrinogen interactions in S. aureus pathogenesis. The binding of octadecane to Sortase A suggests the inhibition of this transpeptidase, which is crucial for bacterial virulence

factor display (Mazmanian et al. 1999); its inhibition could impair pathogenesis (Abujubara et al. 2023). The poor binding of dimethyl disulfide suggests that it is unlikely to be effective. The structure-activity relationship provides insights into drug design targeting these proteins.

ADMET properties of the tested compounds suggest varying potentials for activity and membrane permeability. Ethyl 2-methylbutanoate, with high hydrogen bond acceptors (HBA) and donors (HBD), indicates good solubility and potential for hydrogen bonding. However, its elevated topological polar surface area (TPSA) can hinder diffusion across membranes, affecting bioavailability. This aligns with the observation that increased polarity can impede permeability (Kenny 2022). The high lipophilicity and rotatable bonds of octadecane suggest that it may readily interact with hydrophobic environments, such as membranes; however, its poor solubility could limit absorption. Compounds with high lipophilicity often require formulation strategies to enhance their bioavailability (Argikar et al. 2022). Indole and 2,5-dimethylpyrazine, which have low TPSA values, likely have improved membrane permeability, aiding intracellular activity. These findings underscore the complex interplay of molecular characteristics in determining the pharmacokinetic and safety profiles.

The color change during AgNP synthesis indicated successful reduction, consistent with previous microbial biosynthesis studies. The UV-vis absorption peak at 445 nm matches the reported values for spherical silver nanoparticles, typically around 400 nm. The blue shift suggests a decrease in the particle size, which is consistent with Mie theory. SEM analysis confirmed the uniform distribution of nanoparticles, supporting the synthesis potential of *B. aerius PMRU2.8*. These findings align with studies highlighting microbial synthesis as an eco-friendly nanoparticle production method (Danischewski et al. 2023, Panariello et al. 2020, Rasskazov et al. 2020). The superior antibacterial efficacy of silver nanoparticles compared to the crude extract is due to their nanoscale dimensions and enhanced properties. Larger inhibition zones by SNPs at lower concentrations (25 µg versus 100 µg) align with Rai et al. (2012) and Dakal et al. (2016), who established that increased surface area to volume ratio facilitates efficient bacterial cell membrane interactions through electrostatic attraction and penetration.

The exceptional susceptibility of Enterococcus faecalis to SNPs (99.2% inhibition relative to streptomycin) is significant given its increasing antibiotic resistance. Ultrastructural studies suggest that gram-positive bacteria may experience more severe cell wall disruption from silver nanoparticles due to their peptidoglycan architecture. The pronounced inhibition of Klebsiella pneumoniae (86.7%) by SNPs indicates promising activity against a critical respiratory pathogen. Varying susceptibility patterns across bacterial species likely reflect differences in cell envelope composition, efflux pump mechanisms, and intrinsic resistance determinants, as documented by Hogan et al.(2024) and Suma et al.(2023). The sensitivity

Table 8: Mechanisms of action of key compounds in bacterial inhibition.

Compound	Molecular Target	Proposed Mechanism of Action	Potential Antimicrobial Effect	Reference
Indole	CMP-Kdo synthetase (Gram-negative bacteria)	Strong binding affinity, interference with lipopolysaccharide biosynthesis	Compromised cell wall integrity in Gram-negative bacteria	(Nitulescu et al. 2021)
Indole	Clumping Factor A (S. aureus)	Strong binding affinity, disruption of bacterial adherence	Inhibited biofilm formation and colonization	(Claes et al. 2017)
Octadecane	Sortase A	Inhibition of this transpeptidase enzyme	Impaired display of virulence factors on the bacterial cell surface	(Alharthi et al. 2021)
Octadecane	Cell membrane	Compromise of membrane integrity due to high lipophilicity	Membrane destabilization and potential cell death	(Kolaričet al. 2021)
5-Methyl-2-hexanone	Cell membrane	Disruption of membrane integrity	Particularly effective against S. aureus and K. pneumoniae	-
3-Methylbutanoic acid	Cytoplasm and cell membrane	Cytoplasmic acidification and membrane damage	Disruption of cellular homeostasis	(Ketchamet al. 2022)
Ethyl 2-methylbutanoate	Multiple targets	Enhanced solubility and hydrogen bonding potential (high HBA/HBD)	Broad interaction with cellular components, limited by higher TPSA	(Riel et al. 2019)
Dimethyl disulfide	Multiple targets	Poor binding affinity demonstrated in molecular docking	Limited antibacterial efficacy predicted	-
2,5-Dimethylpyrazine	Cell membrane	Improved membrane permeability (low TPSA)	Enhanced intracellular activity	-

of Vibrio sp. to the crude extract rather than SNPs presents an intriguing counterpoint, possibly explained by specific bioactive compounds targeting Vibrio-specific pathways. Raza et al. (2016) elucidated multiple antimicrobial mechanisms for SNPs, including ROS generation, protein denaturation, and DNA replication inhibition, which may be differentially effective depending on bacterial characteristics. The differential efficacy between gram-positive and gram-negative bacteria could be attributed to variations in cell wall permeability, as suggested by the statistical significance ($p<0.001$) in treatment responses. The F-values (E=42.175, S=37.404, P=17.921) indicate substantial variance between treatment groups, supporting the hypothesis that nanoparticle-mediated antibacterial activity involves multiple targets and mechanisms. The broad-spectrum activity of *B. aerius* PMRU2.8-derived SNPs against clinically relevant pathogens indicates promising applications in developing novel antimicrobial formulations. These findings underscore the complex interplay between nanoparticle characteristics, bacterial physiology, and antimicrobial response. The mechanism of action of each compound in the inhibition of pathogenic bacteria is summarized in Table 8.

The differential decolorization efficacy across four azo dyes is due to their structural characteristics and enzymatic systems in strain PMRU2.8. Superior decolorization of Direct Blue 6 (92.5%) aligns with Guo et al. (2021), who noted di-azo-linked naphthol groups are susceptible to bacterial azo-reductase. Sudan Black and Disperse Red 1 showed Substantial decolorization (91.9% and 86.2%), suggesting the possibility of multiple azo-reductase enzymes. Priyanka et al. (2022) suggest that oxidative enzymes like laccase contribute to decolorization, explaining the ability to degrade diverse azo compounds. Lower decolorization for Brilliant Green (65.3%) is due to its triphenylmethane structure, which resists azo-reductase cleavage. Wanyonyi et al. (2017) reported that triphenylmethane dye decolorization relies more on peroxidase activity, limited in Bacillus species. The time-dependent decolorization suggests an adaptation period for bacterial cells to induce enzymatic machinery (Eskandari et al. 2019). The acceleration between 18-36 h suggests upregulation of enzymes or optimal metabolic conditions. Higher ADR values for Sudan Black (2.13 mg L^{-1}) suggest the enzymatic systems may have evolved preferential activity toward certain azo dye structures. Near-complete decolorization (>90%) for Direct Blue 6 and Sudan Black demonstrates *B. aerius* PMRU2.8's bioremediation potential for textile effluent treatment.

Enhanced cytotoxicity of silver nanoparticles (AgNPs) compared to the ethyl acetate extract (EAE) of *B. aerius* PMRU2.8 is due to their unique properties that increase cellular interactions. Akter et al. (2017) and Liao & Tjong (2019) noted AgNPs are internalized by cells through mechanisms like scavenger receptor-mediated phagocytosis and lipid-raft-mediated endocytosis. Piao et al. (2011) showed AgNPs can localize in the cytoplasm and reach the nucleus, potentially interfering with DNA replication. This may explain the lower LC50 value (310 µg/mL) for AgNPs compared to the extract (548.6 µg.mL^{-1}). A key mechanism of AgNP toxicity is intracellular dissolution, releasing silver ions (Ag+). Akter et al. (2017) and Liao & Tjong (2019) emphasized that these ions are central to AgNP toxicity, interacting with proteins, enzymes, and nucleic acids. Continuous release of silver ions creates a sustained cytotoxic effect not seen with conventional extracts. AgNP cytotoxicity involves oxidative stress pathways. Hackenberg et al. (2011) reported that AgNPs generate reactive oxygen species (ROS) and suppress glutathione levels, causing oxidative imbalance and damage to cellular components. This contributes to their greater cytotoxic potency in the brine shrimp lethality assay. The cytotoxicity pattern suggests potential biomedical applications, particularly in anticancer agent development, but raises concerns about environmental and human safety, necessitating comprehensive toxicological assessments before practical applications.

Study Limitations and Future Directions

While this study provides insights into *B. aerius PMRU2* antimicrobial properties and dye decolorization capabilities of B. aerius PMRU2.8, certain aspects warrant further investigation. Cytotoxicity assessment can be complemented with mammalian cell line testing for clinical applications. Although B. aerius PMRU2.8 demonstrated stability, long-term studies across generations would strengthen its industrial applicability. The azo dye biodegradation assay showed high decolorization rates in this study. Future research should investigate enzymatic pathways in dye degradation, focusing on azo-reductase and oxidative enzymes. Pilot-scale studies using textile effluents would better reflect the industrial applications. Field testing would validate the real-world efficacy. Molecular docking analyses provide mechanistic hypotheses that can be validated through enzyme inhibition assays. Such studies would build upon the findings of novel antimicrobial development. Future investigations should explore the metabolic fate of degraded intermediates, scale-up parameters, and immobilized systems for continuous treatment. The multifunctionality of B. aerius PMRU2.8 suggests its potential as a versatile bioremediation agent, meriting further study.

CONCLUSIONS

This study elucidated the antibacterial efficacy of *Bacillus aerius PMRU2.8*, isolated from marine red algae, against human pathogens. Molecular and biochemical analyses

confirmed its taxonomic identity. Both the ethyl acetate extract and silver nanoparticles exhibited antibacterial activity, with the latter showing enhanced potency. Strain PMRU2.8 also displayed azo dye degradation capabilities, indicating its potential for environmental remediation. The brine shrimp lethality bioassay revealed the cytotoxicity profile of AgNPs, suggesting promising biomedical applications. These findings open avenues for future commercial nanoformulations incorporating PMRU2.8-derived compounds as antimicrobial agents in healthcare. The robust dye degradation ability of this strain positions it for scale-up in environmental pilot studies targeting textile effluent treatment. Additionally, synthetic biology approaches can enhance the production of key bioactive compounds and optimize enzymatic pathways for improved bioremediation efficiency. The multifunctional capabilities of B. aerius PMRU2.8 present significant potential for addressing both clinical antimicrobial resistance and environmental pollution challenges through sustainable biotechnological applications in the future.

REFERENCES

Abujubara, H., Hintzen, J., Rahimi, S., Mijakovic, I., Tietze, D. and Tietze, A., 2023. Substrate-derived sortase A inhibitors: Targeting an essential virulence factor of gram-positive pathogenic bacteria. *Chemical Science*, 14, pp.6975–6985. [DOI]

Akter, M., Sikder, M., Rahman, M., Ullah, A., Hossain, K., Banik, S., Hosokawa, T., Saito, T. and Kurasaki, M., 2017. A systematic review on silver nanoparticles-induced cytotoxicity: Physicochemical properties and perspectives. *Journal of Advanced Research*, 9, pp.1–16. [DOI]

Alharthi, S., Alavi, S., Moyle, P. and Ziora, Z., 2021. Sortase A (SrtA) inhibitors as an alternative treatment for superbug infections. *Drug Discovery Today*, 26, pp.1234–1245. [DOI]

Argikar, U., Blatter, M., Bednarczyk, D., Chen, Z., Cho, Y.S., Doré, M., Dumouchel, J.L., Ho, S., Hoegenauer, K., Kawanami, T. and Mathieu, S., 2022. Paradoxical increase of permeability and lipophilicity with the increasing topological polar surface area within a series of PRMT5 inhibitors. *Journal of Medicinal Chemistry*, 65(18), pp.12386–12402.

Bauer, A.W., Kirby, W.M.M., Sherris, J.C. et al., 1966. Antibiotic susceptibility testing by a standardized single disk method. *American Journal of Clinical Pathology*, 45, pp.493–496. [DOI]

Bhagat, K., Bhagat, J., Gupta, M., Singh, J., Gulati, H., Singh, A., Kaur, K., Kaur, G., Sharma, S., Rana, A., Singh, H., Sharma, S. and Bedi, P., 2019. Design, synthesis, antimicrobial evaluation, and molecular modeling studies of novel indolinedione–coumarin molecular hybrids. *ACS Omega*, 4, pp.8720–8730. [DOI]

Brito, T.L., Campos, A.B., Bastiaan von Meijenfeldt, F.A., Daniel, J.P., Ribeiro, G.B., Silva, G.G. et al., 2018. The gill-associated microbiome is the main source of wood plant polysaccharide hydrolases and secondary metabolite gene clusters in the mangrove shipworm *Neoteredo reynei*. *PLoS One*, 13(11), e0200437. [DOI]

Buchanan, R.E. and Gibbons, N.E. (eds), 1974. *Bergey's Manual of Determinative Bacteriology*. 8th Edition. Williams & Wilkins, Baltimore, USA.

Bullock, N.O. and Aslanzadeh, J., 2012. Biochemical profile-based microbial identification systems. In: *Advanced Techniques in Diagnostic Microbiology*. Springer US, Boston, MA, USA, pp.87–121. [DOI]

Butler, M., Gigante, V., Sati, H., Paulin, S., Al-Sulaiman, L., Rex, J., Fernandes, P., Arias, C., Paul, M., Thwaites, G., Czaplewski, L., Alm, R., Lienhardt, C., Spigelman, M., Silver, L., Ohmagari, N., Kozlov, R., Harbarth, S. and Beyer, P., 2022. Analysis of the clinical pipeline of treatments for drug-resistant bacterial infections: Despite progress, more action is needed. *Antimicrobial Agents and Chemotherapy*, 66, pp.1120–1135. [DOI]

Carvalho, M., Albano, H. and Teixeira, P., 2018. In vitro antimicrobial activities of various essential oils against pathogenic and spoilage microorganisms. *Journal of Food Quality and Hazards Control*, 5, pp.41–48. [DOI]

Chakraborty, N., Ghosh, S., Samanta, M., Das, B. and Chattopadhyay, K.K., 2023. Silver nanoparticle decorated perforated graphene: An efficient and low-cost catalyst for hydrogen evolution reaction. *ECS Journal of Solid-State Science and Technology*, 12(10), 101001. [DOI]

Chen, G., An, X., Li, H., Lai, F., Yuan, E., Xia, X. and Zhang, Q., 2021. Detoxification of azo dye Direct Black G by thermophilic *Anoxybacillus* sp. PDR2 and its application potential in bioremediation. *Ecotoxicology and Environmental Safety*, 214, 112084. [DOI]

Claes, J., Liesenborghs, L., Peetermans, M., Veloso, T., Missiakas, D., Schneewind, O., Mancini, S., Entenza, J., Hoylaerts, M., Heying, R., Verhamme, P. and Vanassche, T., 2017. Clumping factor A, von Willebrand factor-binding protein and von Willebrand factor anchor *Staphylococcus aureus* to the vessel wall. *Journal of Thrombosis and Haemostasis*, 15, pp.1009–1019. [DOI]

Dakal, T.C., Kumar, A., Majumdar, R.S. and Yadav, V., 2016. Mechanistic basis of antimicrobial actions of silver nanoparticles. *Frontiers in Microbiology*, 7, pp.1831–1842. [DOI]

Danischewski, J., Donelson, D., Farzansyed, M., Jacoski, E., Kato, H., Lucin, Q. and Roca, M., 2023. Color transferability from solution to solid using silica coated silver nanoparticles. *Langmuir: The ACS Journal of Surfaces and Colloids*, 39, pp.12345–12356. [DOI]

Eskandari, F., Shahnavaz, B. and Mashreghi, M., 2019. Optimization of complete RB-5 azo dye decolorization using novel cold-adapted and mesophilic bacterial consortia. *Journal of Environmental Management*, 241, pp.91–98. [DOI]

Fernandez-Calvo, A., Reifs, A., Saa, L., Cortajarena, A., De Sancho, D. and Perez-Jimenez, R., 2024. The strongest protein binder is surprisingly labile. *Protein Science: A Publication of the Protein Society*, 33, pp.1120–1132. [DOI]

Ganesh, V.K., Rivera, J.J., Smeds, E., Ko, Y.P., Bowden, M.G., Wann, E.R., Gurusiddappa, S., Fitzgerald, J.R. and Höök, M., 2008. A structural model of the *Staphylococcus aureus* ClfA–fibrinogen interaction opens new avenues for the design of anti-staphylococcal therapeutics. *PLoS Pathogens*, 4(11), e1000226.

Gao, Y., Feng, X., Xian, M., Wang, Q. and Zhao, G., 2018. Inducible expression of anti-CMP-Kdo synthetase (CKS) single-chain antibodies in pathogenic bacteria causes severe growth inhibition. *Frontiers in Microbiology*, 9, pp.83–92.

Ghodake, G., Kim, M., Sung, J., Shinde, S., Yang, J., Hwang, K. and Kim, D., 2020. Extracellular synthesis and characterization of silver nanoparticles—antibacterial activity against multidrug-resistant bacterial strains. *Nanomaterials*, 10, pp.203–214. [DOI]

Gu, X., Cao, Z., Zhao, L., Seswita-Zilda, D., Zhang, Q., Fu, L. and Li, J., 2023. Metagenomic insights reveal the microbial diversity and associated algal polysaccharide-degrading enzymes on the surface of red algae among remote regions. *International Journal of Molecular Sciences*, 24(13), 11019. [DOI]

Guo, G., Liu, C., Hao, J., Tian, F., Ding, K., Zhang, C., Yang, F., Liu, T., Xu, J. and Guan, Z., 2021. Development and characterization of a halo-thermophilic bacterial consortium for decolorization of azo dye. *Chemosphere*, 272, 129916. [DOI]

Hackenberg, S., Scherzed, A., Kessler, M., Hummel, S., Technau, A., Froelich, K., Ginzkey, C., Koehler, C., Hagen, R. and Kleinsasser, N., 2011. Silver nanoparticles: Evaluation of DNA damage, toxicity and

functional impairment in human mesenchymal stem cells. *Toxicology Letters*, 203, pp.27–33. [DOI]

Hogan, A., Motnenko, A., Rahman, A. and Cardona, S., 2024. Cell envelope structural and functional contributions to antibiotic resistance in *Burkholderia cenocepacia*. *Journal of Bacteriology*, 206, pp.1120–1134. [DOI]

Huang, L.R., Ling, X.N., Peng, S.Y., Tan, M.H., Yan, L.Q., Liang, Y.Y., Li, G.H. and Li, K.T., 2023. A marine lipopeptides-producing *Bacillus amyloliquefaciens* HY2-1 with a broad-spectrum antifungal and antibacterial activity and its fermentation kinetics study. *World Journal of Microbiology and Biotechnology*, 39(8), p.196. [DOI]

Jamil, I., Ahmad, F., Khan, M.I., Shanableh, A., Farooq, N., Anjum, S. and Taj, M.B., 2024. A review of the gold nanoparticles' synthesis and application in dye degradation. *Cleaner Chemical Engineering*, 5, p.100126. [DOI]

Karthikeyan, A., Joseph, A. and Nair, B.G., 2022. Promising bioactive compounds from the marine environment and their potential effects on various diseases. *Journal of Genetic Engineering and Biotechnology*, 20, p.14. [DOI]

Kaur, M., Saini, K.C., Mallick, A. and Bast, F., 2023. Seaweed-associated epiphytic bacteria: Diversity, ecological and economic implications. *Aquatic Botany*, 103698. [DOI]

Kenny, P.W., 2022. Hydrogen-bond donors in drug design. *Journal of Medicinal Chemistry*, 65(21), pp.14261–14275.

Ketcham, A., Freddolino, P. and Tavazoie, S., 2022. Intracellular acidification is a hallmark of thymineless death in *E. coli*. *PLOS Genetics*, 18, pp.1010456–1010465. [DOI]

Kim, Y., Kim, H., Jung, E., Kim, J., Hwang, W., Kang, E., Lee, S., Ha, B., Lee, J. and Park, D., 2012. A novel antibacterial compound from *Siegesbeckia glabrescens*. *Molecules*, 17, pp.12469–12477. [DOI]

Kishor, R., Purchase, D., Saratale, G., Saratale, R., Ferreira, L., Bilal, M., Chandra, R. and Bharagava, R., 2021. Ecotoxicological and health concerns of persistent coloring pollutants of textile industry wastewater and treatment approaches for environmental safety. *Journal of Environmental Chemical Engineering*, 9, 105012. [DOI]

Kolarič, A., Kokot, M., Hrast, M., Weiss, M., Zdovc, I., Trontelj, J., Žakelj, S., Anderluh, M. and Minovski, N., 2021. A fine-tuned lipophilicity/hydrophilicity ratio governs antibacterial potency and selectivity of bifurcated halogen bond-forming NBTIs. *Antibiotics*, 10, pp.862–875. [DOI]

Kranjec, C., Ovchinnikov, K., Grønseth, T., Ebineshan, K., Srikantam, A. and Diep, D., 2020. A bacteriocin-based antimicrobial formulation to effectively disrupt the cell viability of methicillin-resistant *Staphylococcus aureus* (MRSA) biofilms. *NPJ Biofilms and Microbiomes*, 6, pp.110–120. [DOI]

Liao, C., Li, Y. and Tjong, S., 2019. Bactericidal and cytotoxic properties of silver nanoparticles. *International Journal of Molecular Sciences*, 20, pp.449–459. [DOI]

Machado, H., Sonnenschein, E.C., Melchiorsen, J. et al., 2015. Genome mining reveals unlocked bioactive potential of marine Gram-negative bacteria. *BMC Genomics*, 16, pp.158–172. [DOI]

Malanovic, N., Ön, A., Pabst, G., Zellner, A. and Lohner, K., 2020. Octenidine: Novel insights in the detailed killing mechanism of Gram-negative bacteria at a cellular and molecular level. *International Journal of Antimicrobial Agents*, 55, 106146. [DOI]

Mangun, V.V., Sugumaran, R., Yong, W.T.L. and Yusof, N.A., 2023. Dataset of 16S ribosomal DNA sequence-based identification of endophytic bacteria isolated from healthy and diseased Sabah red algae, *Kappaphycus alvarezii*. *Data in Brief*, 51, 109785. [DOI]

Mazmanian, S.K., Liu, G., Ton-That, H. and Schneewind, O., 1999. *Staphylococcus aureus* sortase, an enzyme that anchors surface proteins to the cell wall. *Science*, 285(5428), pp.760–763.

Meyer, B.N., Ferrigni, N.R., Putnam, J.E., Jacobsen, L.B., Nichols, D.E.J. and McLaughlin, J.L., 1982. Brine shrimp: A convenient general bioassay for active plant constituents. *Planta Medica*, 45(05), pp.31–34. [DOI]

Nitulescu, G., Margină, D., Zanfirescu, A., Olaru, O. and Nițulescu, G., 2021. Targeting bacterial sortases in search of anti-virulence therapies with low risk of resistance development. *Pharmaceuticals*, 14, pp.415–426. [DOI]

Paba, G., Ávila, R. and Baldiris, D., 2021. Application of environmental bacteria as potential methods of azo dye degradation systems. *Global Journal of Environmental Science and Management*, 7, pp.131–154. [DOI]

Panariello, L., Radhakrishnan, A., Papakonstantinou, I., Parkin, I. and Gavriilidis, A., 2020. Particle size evolution during the synthesis of gold nanoparticles using in situ time-resolved UV–Vis spectroscopy: An experimental and theoretical study unravelling the effect of adsorbed gold precursor species. *The Journal of Physical Chemistry C*, 124, pp.12345–12358. [DOI]

Petersen, L.E., Kellermann, M.Y. and Schupp, P.J., 2020. Secondary metabolites of marine microbes: From natural products chemistry to chemical ecology. In: Jungblut, S., Liebich, V., Bode-Dalby, M. (eds) *YOUMARES 9 – The Oceans: Our Research, Our Future*. Springer, Cham, pp.101–118. [DOI]

Piao, M., Kang, K., Lee, I., Kim, H., Kim, S., Choi, J., Choi, J. and Hyun, J., 2011. Silver nanoparticles induce oxidative cell damage in human liver cells through inhibition of reduced glutathione and induction of mitochondria-involved apoptosis. *Toxicology Letters*, 201, pp.92–100. [DOI]

Prabhakara, K.H. and Kuehn, S., 2023. Algae drive convergent bacterial community assembly at low dilution frequency. *iScience*, 26(6), pp.106879–106889. [DOI]

Priyanka, J.V., Rajalakshmi, S., Kumar, P.S., Krishnaswamy, V.G., Al Farraj, D.A., Elshikh, M.S. and Gawwad, M.R.A., 2022. Bioremediation of soil contaminated with toxic mixed reactive azo dyes by co-cultured cells of *Enterobacter cloacae* and *Bacillus subtilis*. *Environmental Research*, 204, 112136. [DOI]

Raetz, C.R. and Whitfield, C., 2002. Lipopolysaccharide endotoxins. *Annual Review of Biochemistry*, 71, pp.635–700.

Rai, M.K., Deshmukh, S.D., Ingle, A.P. and Gade, A.K., 2012. Silver nanoparticles: The powerful nano-weapon against multidrug-resistant bacteria. *Journal of Applied Microbiology*, 112(5), pp.841–852. [DOI]

Rasskazov, I., Carney, P. and Moroz, A., 2020. Intriguing branching of the maximum position of the absorption cross section in Mie theory explained. *Optics Letters*, 45(14), pp.4056–4059. [DOI]

Raza, M.A., Kanwal, Z., Rauf, A., Sabri, A.N., Riaz, S. and Naseem, S., 2016. Size- and shape-dependent antibacterial studies of silver nanoparticles synthesized by wet chemical routes. *Nanomaterials*, 6(4), pp.74–85. [DOI]

Riel, A., Rowe, R., Ho, E., Carlsson, A., Rappé, A., Berryman, O. and Ho, P., 2019. Hydrogen bond enhanced halogen bonds: A synergistic interaction in chemistry and biochemistry. *Accounts of Chemical Research*, 52, pp.1234–1245. [DOI]

Shen, C. and Zhang, Y., 2023. Enumeration of bacteria in broth suspension by spread and pour plating. In: *Food Microbiology Laboratory for the Food Science Student: A Practical Approach*. Springer International Publishing, Cham, pp.19–24. [DOI]

Suma, T., Alam, N., Raihan, S., Zahid, M., Mandal, S., Suchana, F., Kundu, R., Hossain, A. and Muhit, M., 2023. Association of antibacterial susceptibility profile with the prevalence of genes encoding efflux proteins in the Bangladeshi clinical isolates of *Staphylococcus aureus*. *Antibiotics*, 12, pp.305–315. [DOI]

Varjani, S., Rakholiya, P., Ng, H., You, S. and Teixeira, J., 2020. Microbial degradation of dyes: An overview. *Bioresource Technology*, 313, 123728. [DOI]

Wanyonyi, W., Onyari, J., Shiundu, P. and Mulaa, F., 2017. Biodegradation and detoxification of Malachite Green dye using novel enzymes from

Bacillus cereus strain KM201428: Kinetic and metabolite analysis. *Energy Procedia*, 119, pp.38–51. [DOI]

Xie, Y., Peng, Q., Ji, Y., Xie, A., Yang, L., Mu, S., Li, Z., He, T., Xiao, Y., Zhao, J. and Zhang, Q., 2021. Isolation and identification of antibacterial bioactive compounds from *Bacillus megaterium* L2. *Frontiers in Microbiology*, 12, pp.645484–645494. [DOI]

Yin, I., Zhang, J., Zhao, I., Mei, M., Li, Q. and Chu, C., 2020. The antibacterial mechanism of silver nanoparticles and its application in dentistry. *International Journal of Nanomedicine*, 15, pp.2555–2562. [DOI]

Zhang, F., Braun, D.R., Chanana, S., Rajski, S.R. and Bugni, T.S., 2019. Phallusialides A–E, pyrrole-derived alkaloids discovered from a marine-derived *Micromonospora* sp. bacterium using MS-based metabolomics approaches. *Journal of Natural Products*, 82(12), pp.3432–3439. [DOI]

Zhang, J., Wang, X., Yan, Y., Jiang, L., Wang, J., Li, B. and Xiang, W., 2010. Isolation and identification of 5-hydroxyl-5-methyl-2-hexenoic acid from *Actinoplanes* sp. HBDN08 with antifungal activity. *Bioresource Technology*, 101(21), pp.8383–8388. [DOI]